Available online at www.sciencedirect.com
ScienceDirect
Comput. Methods Appl. Mech. Engrg. 315 (2017) 881–895
Computer methods in applied mechanics and engineering
www.elsevier.com/locate/cma

Developing a four-dimensional lattice spring model for mechanical responses of solids

Gao-Feng Zhao

State Key Laboratory of Hydraulic Engineering Simulation and Safety, School of Civil Engineering, Tianjin University, Tianjin, 300072, China

Received 22 August 2016; received in revised form 2 November 2016; accepted 30 November 2016
Available online 7 December 2016

Highlights

- The Poisson's ratio limitation of classical LSM is released by introducing an extra fourth-dimensional interaction.
- The method of constructing 4D lattice spring model is presented.
- The method of parameters selection is provided.
- The underlying principle is investigated using hyperelasticity analysis.

Abstract

In this work, a four-dimensional lattice spring model is developed for studying the mechanical responses of solids. Our results indicate that the Poisson's ratio limitation of the classical lattice spring model defined in three-dimensional space can be released by introducing an extra fourth-dimensional interaction. The fourth-dimensional lattice spring model adopts central interactions only, and it can naturally represent the nonlinear dynamic responses of solids without special treatment of rigid body rotation or incremental integration of non-central/non-local interaction as used in the traditional methods. Applicability of the model is illustrated from a few numerical examples.

Keywords: Extra dimension; Lattice spring model; Solids; Poisson's ratio

1. Introduction

Mechanical responses of solids provide important foundations for many scientific disciplines. As examples, Poisson's ratio of materials remains a subject of study in materials science more than two hundred years since its discovery [1], the dynamic fracture of brittle solids is regarded as the key to understanding the mechanism of earthquakes in the geosciences [2], and dynamic large deformation responses of solids are essential in the design and control of new machines such as soft robots in mechanical engineering [3]. With the advancement of computer science, numerical models now provide powerful tools in the study of mechanical responses of solids. The ultimate goal of a numerical model for solid mechanics is to build up virtual solids that can realistically reproduce the responses

E-mail address: gaofeng.zhao@tju.edu.cn.

http://dx.doi.org/10.1016/j.cma.2016.11.034
0045-7825/

of their physical counterparts while maintaining the simplicity of the model. Although many numerical models have been developed, we are still far away from achieving this goal.

Divide and conquer is the most commonly used strategy in the development of numerical models. There are two commonly adopted methodologies. The first is based on the top-to-bottom concept, in which the partial differential equations of the corresponding mechanical problem of solids are first constructed macroscopically and numerical techniques are subsequently used to mathematically solve these equations through spatial discretization of the target, e.g., the finite element method (FEM) [4] and the natural element method (NEM) [5]. Another group of numerical models adopt the bottom-to-top approach, in which the target is divided into a group of small elements and the mechanical responses of the target are mimicked using physically based laws such as Newton's second law and the laws representing the interactions between the corresponding numerical elements. The molecular dynamics (MD) [6] technique that tries to mimic the response of a system based on a group of simulated atoms and/or molecules is the representative one of this kind of approaches. Another well-known model is the discrete element model (DEM) developed by Cundall and Strack [7] to simulate the responses of granular materials using groups of spherical particles. Among these bottom-to-top methodology based models, the lattice spring model developed by Hrennikoff [8] in 1941 is a commonly ignored approach that represents the solid as a group of mass points linked through springs to describe the mechanical responses of solids. This lattice spring model reduces the mechanical problems of solids into a series of 1D interactions. In this sense, it is simple and should be an ideal candidate for building up virtual solids. However, the lattice spring model is intrinsically limited in that it can only solve elastic problems with a fixed Poisson's ratio. Numerous techniques and models have been developed to overcome this limitation, including the Born spring model [9], the beam element model [10], the multibody shear spring [11], and the nonlocal potential [12]. However, introducing noncentral or nonlocal interactions between particles gives rise to additional complex mathematic calculations and incremental integration that might introduce additional sources of accumulative error. All these effects disrupt the simplicity and robustness of the lattice spring model for modelling mechanics problems of solid.

In this work, by utilizing the extra dimension concept, a fourth-dimensional (4D) lattice spring model is developed to overcome the Poisson's ratio limitation of the classical lattice spring model defined in three-dimensional space while still maintaining a purely central interaction to preserve the model's simplicity. Fourth-dimensional interaction is considered on the basis of a hyper-membrane constructed using a parallel world concept. The topological structures of the 4D lattice spring model and selection of material parameters are studied via numerical simulations and hyperelasticity analysis. The obtained results show that the 4D lattice spring model can solve elastic problems with various Poisson's ratios. Moreover, we demonstrate its potential for solving complex solid mechanics problems from a few examples.

2. The model

2.1. Fourth-dimensional lattice model

In classical physics, such as general relativity, there are three spatial dimensions, with time as the fourth dimension. To unify the four fundamental forces in nature, some researchers have proposed five dimensional space-time, e.g., Kaluza–Klein theory (KK theory) [13], in which one extra spatial dimension is introduced. The concept of extra dimension has long been regarded as a fascinating subject in theoretical physics [14]. In this work, inspired by the KK theory, we view solids in 3D space as mappings of hyper-membranes from 4D space. It should be mentioned that our world is three-dimensional from our common sense. Yet, like in the Plato's cave allegory, we cannot prove that the world has extra dimension until we could escape from the cave (our 3D world), which seems impossible. Fortunately, using a computer, a virtual hyper-membrane in 4D can be constructed from a lattice and its responses can be studied through the numerical simulation. Nevertheless, our goal is not to perform a mind test through the computer simulation but rather to construct a lattice model for solving mechanical problems of solids.

A hyper-membrane in 4D space can be easily formed using a parallel world concept by linking an object in the observed 3D space to its parallel version in the fourth dimension. They are closely connected through fourth-dimensional interactions. It is assumed that the original and parallel versions have the same material properties and boundary conditions. The construction process and components of the 4D lattice spring model are illustrated in Fig. 1. As shown in Fig. 1(a), a cubic lattice model in 3D space that can reproduce isotropic elasticity with a fixed Poisson's

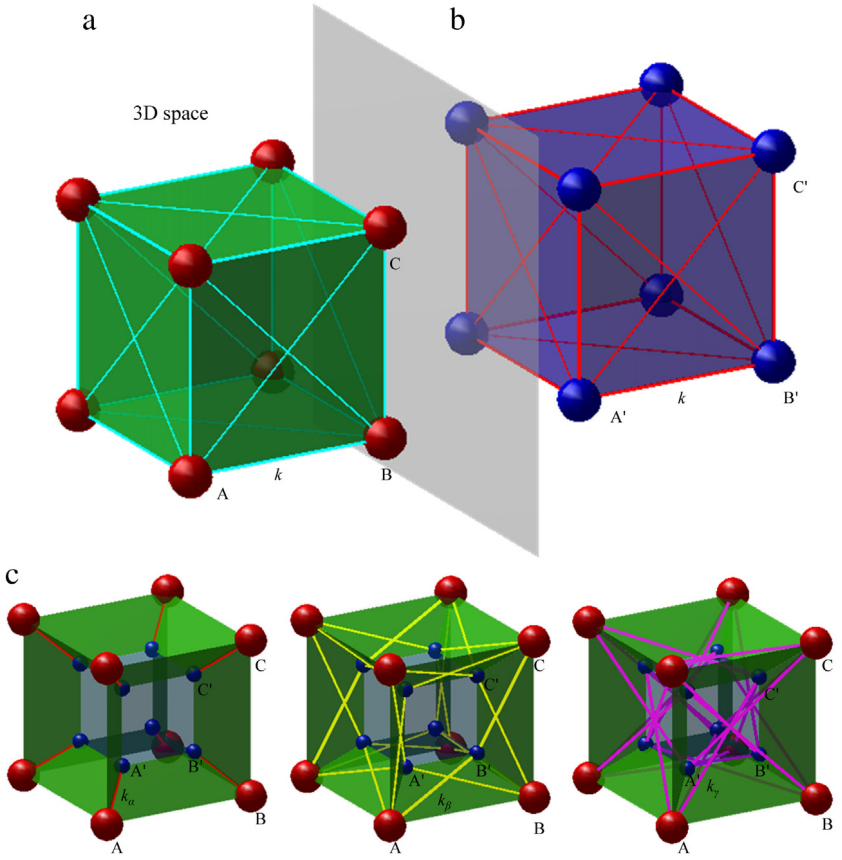

Fig. 1. Generation of a 4D lattice spring model. (a) Original lattice model in 3D space for isotropic elasticity with a fixed Poisson's ratio of 0.25; (b) parallel version in the fourth dimension according to the hyper-membrane assumption; and (c) three types of 4D interactions to link the original lattice model with the parallel model (plotted using a 4D spatial projection method).

ratio of 0.25 is extended to four dimensions. The cubic lattice model is constructed from two types of springs with the same stiffness k: orthotic springs (e.g., AB) and diagonal springs (e.g., AC). Under the hyper-membrane assumption, the 3D lattice model will have its parallel mapped version in the fourth dimension, as shown in Fig. 1(b). The distance between the two models (the original and the parallel) along the fourth dimension is taken as one lattice constant. For a given mass point A, the corresponding parallel version is denoted as A′. The parallel lattice model shares exactly the same connection and spring stiffness of the original model; i.e. both orthotic and diagonal springs will have corresponding parallel versions. The last step for the construction is to connect the original and parallel models using 4D interactions (springs). Here, the rule is that one spring of the original lattice model (e.g., A–B) will generate four corresponding 4D springs: (A–A′), (B–B′), (A–B′) and (B–A′). For a cubic lattice, three types of 4D interactions occur (see Fig. 1(c)). The first interaction is to link the original mass points (A, for example) to its parallel copy (A′) with spring stiffness denoted by k_α. The second type of 4D interaction is formed from the orthotic springs with stiffness denoted by k_β. The third type is formed from diagonal springs with stiffness denoted by k_γ. It is difficult for us to image and draw four-dimensional objects. Fortunately, we can plot the 4D analog (*Tesseract*) of a cube using a standard 4D spatial projection method to help the understanding of a 4D lattice.

The original lattice, the parallel model and 4D interactions (springs) comprise the 4D lattice spring model. Depending on the different configurations of 4D interactions, a number of 4D lattice models can be formed. The most straightforward one is that all 4D interactions (springs) share the same stiffness as expressed by

$$k_\alpha = k_\beta = k_\gamma = \lambda^{4D} k \tag{1}$$

where λ^{4D} is the 4D stiffness ratio and k is the spring stiffness of the original model (referred to as the base spring stiffness). Here, this lattice configuration is called the 4D Lattice (I).

The second version (4D Lattice (II)) is obtained by excluding the third type of 4D interaction from 4D Lattice (I), as can be achieved by setting the stiffness k_γ equal to zero, as expressed by

$$k_\alpha = k_\beta = \lambda^{4D}k, k_\gamma = 0. \tag{2}$$

In the third version, 4D Lattice (III), the motion in the fourth dimension is assumed to be fixed by setting the stiffness of the first type 4D interaction as infinite, expressed as

$$k_\beta = k_\gamma = \lambda^{4D}k, k_\alpha = \infty. \tag{3}$$

Removal of the third 4D interaction from 4D Lattice (III) results in the fourth 4D lattice model (4D Lattice (IV)), expressed as

$$k_\beta = \lambda^{4D}k, k_\gamma = 0, k_\alpha = \infty. \tag{4}$$

These models are the most straightforward 4D lattice configurations; new configurations can be generated by mixing these. For example, rather than directly setting the stiffness of the third type of 4D interaction to zero, a reduction coefficient (3/4) can be assigned, which will result in a modified version of 4D Lattice (I) denoted as 4D Lattice (I-m). The mathematic expression for this lattice is

$$k_\alpha = k_\beta = 4/3k_\gamma = \lambda^{4D}k. \tag{5}$$

These models are described by two parameters: the base spring stiffness k and the 4D stiffness ratio λ^{4D} for the 4D interaction. When $\lambda^{4D} = 0$, the responses of these models will be the same as the original lattice model because there will no longer be any connection between the original and parallel models.

2.2. Interaction and motion equations

In the 4D lattice spring model, the motion of mass points is assumed to satisfy Newton's second law in the time dimension and the interaction between mass points is represented as springs. In this work, the mechanical system of the 4D lattice spring model is solved using the central finite difference scheme [15]. To obtain static solutions, we adopt the local mechanical damping scheme developed for DEM [7].

The motion state of the mass points satisfies Newton's second law and is written simply as

$$\frac{\partial^2 \mathbf{x}}{\partial t^2} = \frac{\mathbf{F}}{m} \tag{6}$$

where $\frac{\partial^2 \mathbf{x}}{\partial t^2}$ is the acceleration of the particle, $\mathbf{F}$ is the particle force induced from the linked springs and body force term, and m is the mass of the particle.

In this work, when an index is used together with a vector symbol (in bold), it refers a vector of the particle with the index; when two indices are used, it represents a vector between two particles with the two indices correspondingly. An example is given as follows. In the 4D lattice spring model, force calculations are based on pair interactions and only involve two particles. The interaction between two particles is given as

$$\mathbf{F}_{ij} = ku_n\mathbf{n}_{ij}. \tag{7}$$

where $\mathbf{F}_{ij}$ is the force from particle i to particle j, $\mathbf{n}_{ij}$ is the normal vector from particle i to particle j, k is the stiffness of the spring and u_n is the deformation of the spring, which is calculated as

$$u_n = \left|\mathbf{x}_j - \mathbf{x}_i\right| - \left|\mathbf{x}_j^0 - \mathbf{x}_i^0\right| \tag{8}$$

where $\mathbf{x}$ is the current position of the mass point, $\mathbf{x}^0$ is the corresponding initial position, and $|\bullet|$ refers to get the normal of a vector. The normal direction is calculated as

$$\mathbf{n}_{ij} = \frac{\mathbf{x}_j - \mathbf{x}_i}{\left|\mathbf{x}_j - \mathbf{x}_i\right|}. \tag{9}$$

2.3. Parameters identification

The 4D lattice spring model can be regarded as a virtual solid characterized by two parameters: the base spring stiffness k and the 4D stiffness ratio λ^{4D}. Because the purpose of the model is to provide a numerical tool for modelling the mechanical response of solids in engineering applications, parameter identification is conducted to link the two mechanical parameters of the model to two commonly used elastic constants: the elastic modulus and the Poisson's ratio. In this work, a general procedure based on numerical simulations is used. As shown in Fig. 2(a), a virtual uniaxial compression test is conducted for a cube with $20 \times 20 \times 20$ particles using the 4D lattice spring model. During the calculation, the Poisson's ratio and elastic modulus are obtained according to their corresponding definitions.

A nonlinear relationship can be obtained between the Poisson's ratio and the 4D stiffness ratio given by

$$\lambda_{4D} = f(v). \tag{10}$$

This equation can be determined using nonlinear fitting of the corresponding numerical results; for example, for the 4D Lattice (I-m) model, the following polynomial equation is obtained:

$$\lambda_{4D} = -211.13493779v^3 + 162.84655851v^2 - 55.42449719v + 6.92902211. \tag{11}$$

Eq. (11) indicates that, for a given Poisson's ratio, the corresponding 4D stiffness ratio can be determined. The elastic modulus obtained from numerical simulation is scaled with the lattice model in 3D space ($\lambda_{4D} = 0$) and is termed the elastic modulus increase ratio. Generally, linear relationships are observed between the 4D stiffness ratio and the elastic modulus increase ratio (see Fig. 2(c)). The elastic modulus increase ratio under a given 4D stiffness ratio can also be represented as

$$\eta = g(\lambda_{4D}). \tag{12}$$

For better fitting, a high-order function can be used; e.g., in this work, a second-order polynomial equation is obtained for the 4D Lattice (I-m) model:

$$\eta = -0.0078506\lambda_{4D}^2 + 0.41613615\lambda_{4D} + 1.00369223. \tag{13}$$

Now, for a given elastic modulus E and Poisson's ratio v, the procedure for calculating the lattice parameters is as follows. The first step is to obtain the 4D stiffness ratio using Eq. (10) with the input Poisson's ratio. Then, with the calculated 4D stiffness ratio, the elastic modulus increase ratio can be obtained using Eq. (12). For the 3D lattice spring model ($\lambda_{4D} = 0$), the corresponding relationship between the elastic modulus (at a Poisson's ratio of 0.25) and spring stiffness k_{3d} can be obtained by using a strain energy equivalent concept expressed as [11]

$$k_0 = \frac{6VE}{\sum l_i^2} \tag{14}$$

where k_{3d} is the spring stiffness, E is the elastic modulus, V is the volume of the model in 3D, and l_i is the length of the ith spring. In the theoretical analysis, V is the representative volume and k_0 is independent from the volume. However, in the numerical simulation, V is the representing volume of the lattice model that could have arbitrary shapes. Eq. (14) is obtained from a strain energy equivalent method. More details can be found in [11]. From Eqs. (13) and (14), the corresponding base spring stiffness for the 4D model is obtained as

$$k = \frac{6VE}{\eta \sum l_i^2}. \tag{15}$$

2.4. Hyperelasticity analysis

In this section, the ability of the 4D lattice spring model to represent a variety of Poisson's ratios will be further investigated using hyperelasticity analysis. First, we assume that the hyper-membrane made up from springs is spatially isotropic in 3D space and is homogeneous along the fourth dimension. When the small

deformation assumption is applicable, the corresponding elastic matrix of the membrane can be obtained by using the hyperelasticity analysis (Eq. (26)), which can be represented using four elastic constants as

$$\Omega = \begin{bmatrix} C1 & C2 & C2 & C4 & 0 & 0 & 0 & 0 & 0 & 0 \\ C2 & C1 & C2 & C4 & 0 & 0 & 0 & 0 & 0 & 0 \\ C2 & C2 & C1 & C4 & 0 & 0 & 0 & 0 & 0 & 0 \\ C4 & C4 & C4 & C3 & 0 & 0 & 0 & 0 & 0 & 0 \\ 0 & 0 & 0 & 0 & C2 & 0 & 0 & 0 & 0 & 0 \\ 0 & 0 & 0 & 0 & 0 & C2 & 0 & 0 & 0 & 0 \\ 0 & 0 & 0 & 0 & 0 & 0 & C2 & 0 & 0 & 0 \\ 0 & 0 & 0 & 0 & 0 & 0 & 0 & C4 & 0 & 0 \\ 0 & 0 & 0 & 0 & 0 & 0 & 0 & 0 & C4 & 0 \\ 0 & 0 & 0 & 0 & 0 & 0 & 0 & 0 & 0 & C4 \end{bmatrix}. \tag{16}$$

Due to the membrane made from springs with central interaction only, the shear component of matrix (e.g. $\Omega(5,5)$) is equal to its off-diagonal component (e.g. $\Omega(1,2)$).

Applying the stress free boundary condition along the fourth dimension, we can further write Eq. (16) as

$$\begin{pmatrix} \sigma_{11} \\ \sigma_{22} \\ \sigma_{33} \\ \sqrt{2}\sigma_{12} \\ \sqrt{2}\sigma_{23} \\ \sqrt{2}\sigma_{13} \end{pmatrix} = D1 \begin{bmatrix} 1 & \frac{D2}{D1} & \frac{D2}{D1} & 0 & 0 & 0 \\ \frac{D2}{D1} & 1 & \frac{D2}{D1} & 0 & 0 & 0 \\ \frac{D2}{D1} & \frac{D2}{D1} & 1 & 0 & 0 & 0 \\ 0 & 0 & 0 & \frac{D3}{D1} & 0 & 0 \\ 0 & 0 & 0 & 0 & \frac{D3}{D1} & 0 \\ 0 & 0 & 0 & 0 & 0 & \frac{D3}{D1} \end{bmatrix} \begin{pmatrix} \varepsilon_{11} \\ \varepsilon_{22} \\ \varepsilon_{33} \\ \sqrt{2}\varepsilon_{12} \\ \sqrt{2}\varepsilon_{23} \\ \sqrt{2}\varepsilon_{13} \end{pmatrix} \tag{17}$$

where

$$D1 = C1 - \frac{C4C4}{C3} \tag{18}$$

$$D2 = C2 - \frac{C4C4}{C3} \tag{19}$$

$$D3 = C2. \tag{20}$$

Comparing Eq. (17) with the classical elastic matrix of isotropic elasticity, we can introduce two Poisson's ratios:

$$v' = \frac{D2}{D1 + D2} \tag{21}$$

$$v'' = \frac{2D3 - D1}{2D3 - 2D1} \tag{22}$$

where v' refers to the Poisson's ratio related to the bulk response and v'' is related to the shear response. Theoretical analysis of the Poisson's ratios of the 4D lattice spring models can be conducted by extending the hyperelasticity analysis procedure developed by Gao and Klein [16] which was also used by Zhang and Ge [17]. First, we assume that a uniform strain deformation specified by ε_{ij} $(i, j = 1, 2, 3, 4)$ is applied to the lattice model. Under the small deformation assumption, the spring's deformation can be represented as

$$u_n = \xi_i \varepsilon_{ij} \xi_j \tag{23}$$

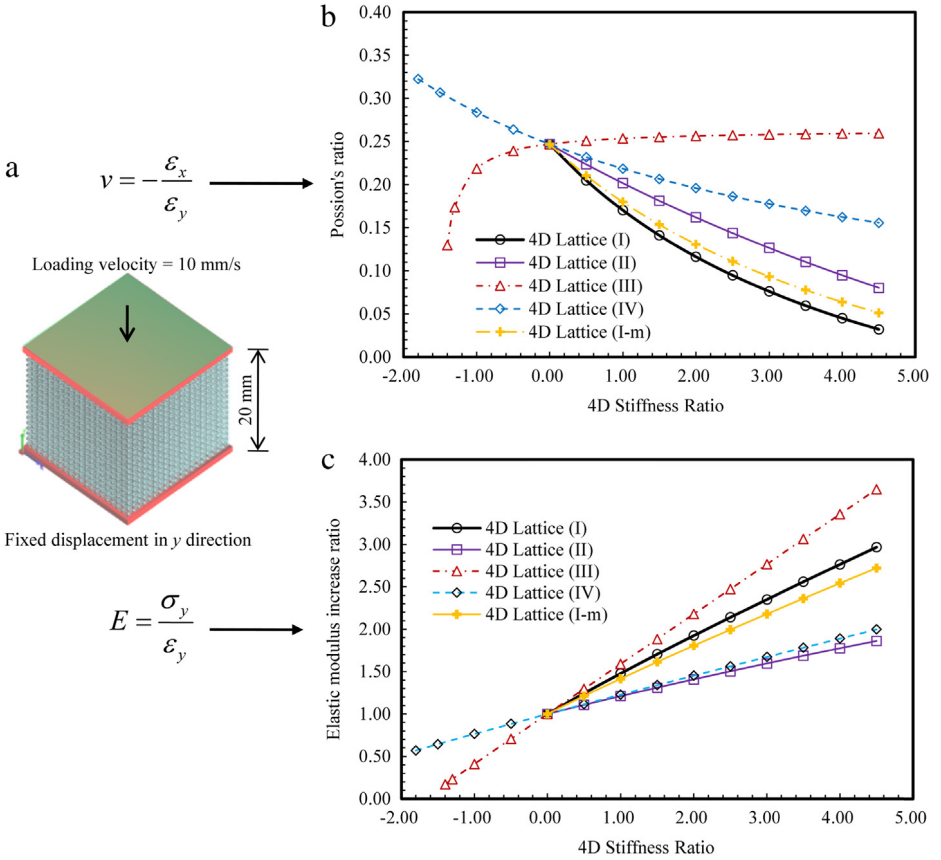

Fig. 2. Relationship between the 4D stiffness ratio λ^{4D} and elastic constants obtained from numerical simulation of a uniaxial compression test: (a) computational model (strain and stress are calculated from average force/displacement values of the corresponding cubic specimen surfaces), (b) relationship between λ^{4D} and the Poisson's ratio, and (c) relationship between λ^{4D} and the elastic modulus increase ratio.

where ξ is the component of the spring's normal vector $\mathbf{n}$. The strain energy stored in the spring is then expressed as

$$U = \frac{1}{2} k l^2 \xi_i \varepsilon_{ij} \xi_j. \tag{24}$$

The total energy stored in per unit volume of the hyper-membrane is

$$\Phi = \frac{2\sum U_{3D} + \sum U_\alpha + \sum U_\beta + \sum U_\gamma}{V\Delta} \tag{25}$$

where V is the volume of the hyper-membrane in 3D space and Δ is the thickness in the fourth dimension. According to hyperelasticity theory, the elastic matrix tensor can be expressed as

$$C_{ijnm} = \frac{\partial^2 \Phi}{\partial \varepsilon_{ij} \partial \varepsilon_{nm}}. \tag{26}$$

For a given lattice model, the corresponding elastic constants can be determined from Eq. (26); the Poisson's ratios can then be obtained using Eqs. (21) and (22). In the following, both the cubic 4D lattice model and the 4D random lattice model are investigated. Because the Poisson's ratio is the main concern, the base spring stiffness k is taken as one to simplify the derivation. For 4D interactions, the corresponding stiffness is taken as a ratio between k, which leads the calculation as dimensionless. Using Eq. (26), for a cubic lattice with $N \times N \times N$ mass points in original

space, we can derive the corresponding elastic constants for the 4D lattice model as

$$C1 = 4N(N-1)^2 + 2N^2(N-1) + N^2(N-1)k_\beta + \frac{8N(N-1)^2 k_\gamma}{3} \tag{27}$$

$$C2 = 2N(N-1)^2 + \frac{4N(N-1)^2 k_\gamma}{3} \tag{28}$$

$$C3 = N^3 k_\alpha + 3N^2(N-1)k_\beta + 4N(N-1)^2 k_\gamma \tag{29}$$

$$C4 = N^2(N-1)k_\beta + \frac{8N\,(N-1)^2\,k_\gamma}{3}. \tag{30}$$

Using these equations, and taking $N \to \infty$, we obtain the corresponding Poisson's ratios as

$$v' = \frac{18k_\alpha + 54k_\beta + 72k_\gamma + 12k_\alpha k_\gamma - 12k_\beta k_\gamma - 9k_\beta k_\beta - 16k_\gamma k_\gamma}{72k_\alpha + 216k_\beta + 288k_\gamma + 9k_\alpha k_\beta + 36k_\alpha k_\gamma + 48k_\beta k_\gamma + 9k_\beta k_\beta + 16k_\gamma k_\gamma} \tag{31}$$

$$v'' = \frac{18k_\alpha + 54k_\beta + 72k_\gamma + 9k_\alpha k_\beta - 12k_\beta k_\gamma + 18k_\beta k_\beta - 64k_\gamma k_\gamma}{72k_\alpha + 216k_\beta + 288k_\gamma + 18k_\alpha k_\beta + 24k_\alpha k_\gamma + 48k_\beta k_\gamma + 36k_\beta k_\beta - 32k_\gamma k_\gamma}. \tag{32}$$

From observation, $v' = v''$ when $k_\gamma = 3/4k_\beta$, which is why the 4D Lattice (I-m) model can reproduce the isotropic elastic responses.

Models with a general random lattice structure can also be easily extended to the 4D space using the same procedure as that used for the cubic lattice model, except that no distinction is made between the second and third types of 4D interactions, i.e. $k_\beta = k_\gamma$. The corresponding four elastic constants for a 4D random lattice are calculated as

$$C1 = \frac{2}{L^3\Delta}\int_{l_1}^{l_2}\int_0^{2\pi}\int_0^{\pi}\left(l^2 + \frac{l^4}{l^2+\Delta^2}k_\beta\right)(\sin\theta)^5\cos\varphi^4\frac{N\,(l)}{2\pi}d\theta d\phi dl \tag{33}$$

$$C2 = \frac{2}{L^3\Delta}\int_{l_1}^{l_2}\int_0^{2\pi}\int_0^{\pi}\left(l^2 + \frac{l^4}{l^2+\Delta^2}k_\beta\right)(\sin\theta)^5\,(\cos\varphi)^2\,(\sin\varphi)^2\,\frac{N(l)}{2\pi}d\theta d\phi dl \tag{34}$$

$$C3 = \frac{2}{L^3\Delta}\int_{l_1}^{l_2}\int_0^{2\pi}\int_0^{\pi}\left(\frac{1}{L_N}\Delta^2 k_\alpha + \frac{1}{l^2+\Delta^2}k_\beta\right)\frac{N\,(l)}{2\pi}\sin\,(\theta)\,d\theta d\phi dl \tag{35}$$

$$C4 = \frac{2}{L^3\Delta}\int_{l_1}^{l_2}\int_0^{2\pi}\int_0^{\pi}\frac{l^2}{l^2+\Delta^2}\,(\sin\theta)^3\,(\sin\varphi)^2\,k_\beta\frac{N(l)}{2\pi}d\theta d\phi dl \tag{36}$$

where L is the length of a sufficiently large cube with a large number of particles, θ and ϕ refer to the spherical coordinates of the springs in the 3D spatial space being transformed from a Cartesian coordinate system to a spherical system, l refers to the spring's length and the number of springs assumed to be uniformly distributed from l_1 to l_2, L_N is the lattice number, which is defined as the mean number of springs linked to per mass particle, and $N(l)$ is the density of springs with length l. The corresponding Poisson's ratios for a random lattice were obtained using the above equations. We found that the 4D random lattice model produces isotropic elastic responses directly.

Fig. 3 shows the results of the Poisson's ratios calculated from the hyperelasticity analysis and the numerical simulation. In the hyperelasticity analysis, a Poisson's ratio larger than 0.25 is produced with negative 4D stiffness ratios. However, the corresponding lattice spring model with negative 4D stiffness ratio may be physically unstable, which is why the 4D Lattice (I-m) cannot be applied when the Poisson's ratio is greater than 0.25. For the 4D random lattice model, lattice models with different lattice numbers (L_N) are generated by setting different threshold values for spring generation between particles. Two random lattice models with $L_N = 8.4$ and 13.2 were generated; the numerical simulation results for recovering the Poisson's ratio are shown in Fig. 3. The Poisson's ratio of a 4D random lattice with low L_N differs from that obtained via hyperelasticity analysis, and the reproduced Poisson's ratio is greater than 0.25. The reason for this different Poisson's ratio is that the homogeneous deformation assumption in the hyperelasticity analysis is no longer applicable for the random lattice model with low L_N.

Although a spring with negative stiffness, e.g., a gravitation-like interaction, is intrinsically unstable, when placed into a stiff system such as the 4D Lattice (IV) model, such a spring can become physically stable. Numerical

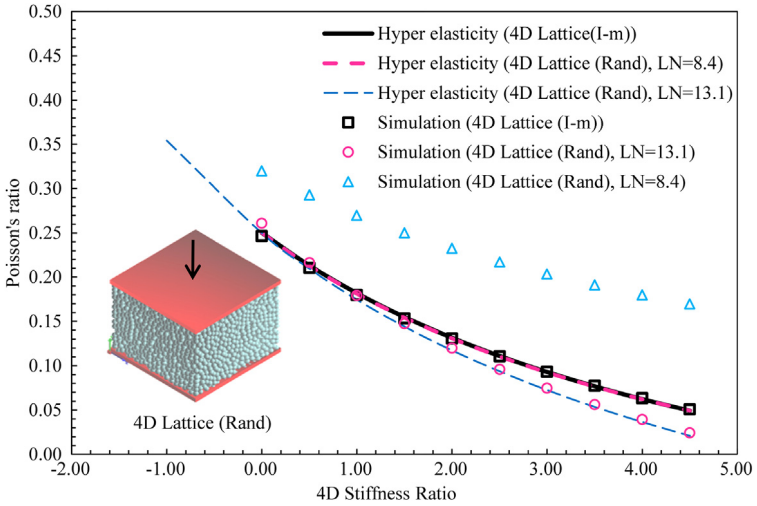

Fig. 3. Poisson's ratios predicted by hyperelasticity analysis and by numerical simulation using the 4D lattice spring model.

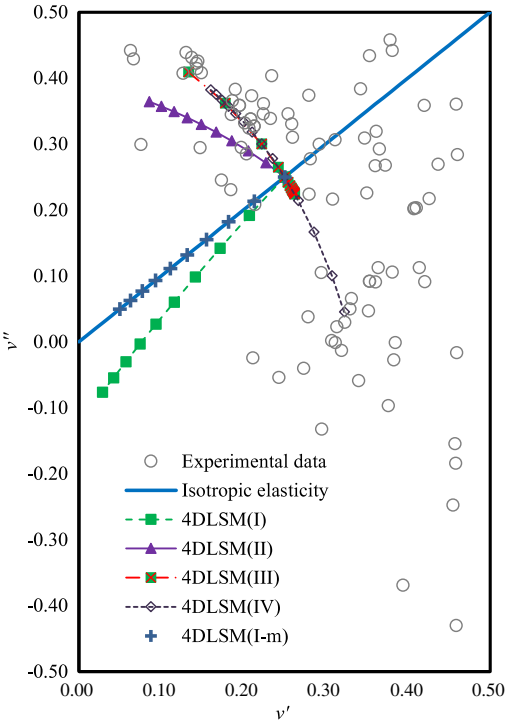

Fig. 4. Poisson's ratios of cubic lattice models calculated from hyperelasticity analysis ($k_\alpha \in [-4, 5]$, $k_\beta \in [-4, 5]$, and $k_\gamma \in [-4, 5]$); experimental data for cubic crystals [18] are also shown.

simulation is the direct method for determining whether a model is stable. For this reason, a numerical-simulation-based procedure is recommended to identify the corresponding model parameters for the 4D lattice spring model rather than using hyperelasticity theory.

In the case of cubic crystals, three elastic constants are identical to the elastic constants of the hyper-membrane mapped in 3D space. The experimental data for 92 cubic crystals [18] were processed using Eqs. (21) and (22) to calculate the corresponding Poisson's ratios; the results are shown in Fig. 4.

The display range was fixed to [0, 0.5] for the x-axis and to [-0.5, 0.5] for the y-axis to filter out abnormal values; this range covers 97.8% of the experimental data points. The results of the corresponding hyperelasticity analysis and

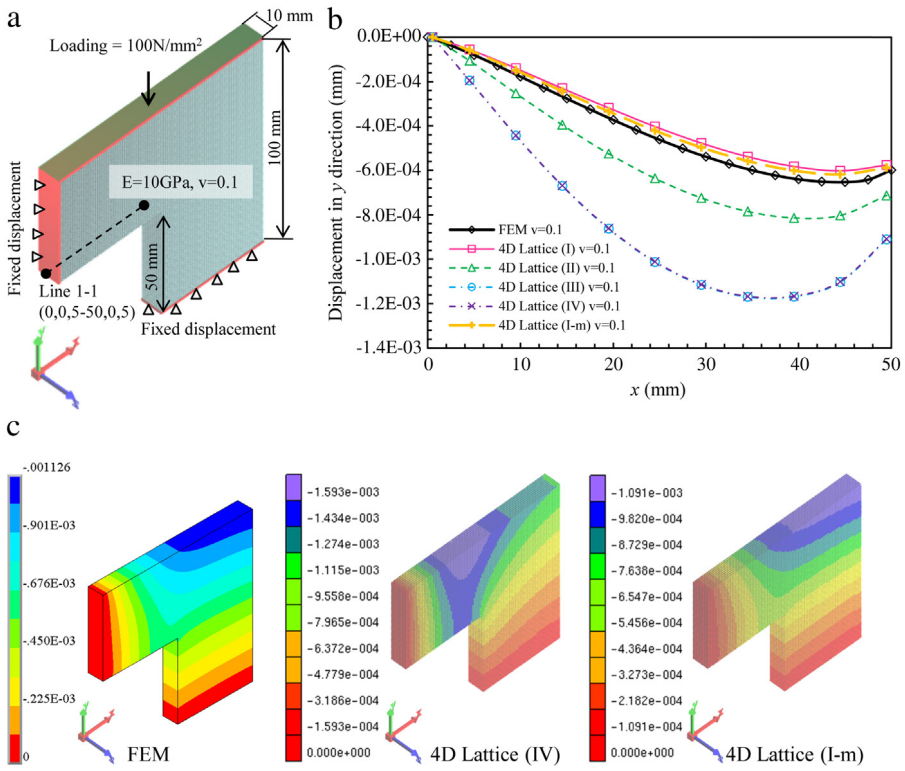

Fig. 5. Boundary value problem with complex geometry domain solved by the 4D lattice spring model and FEM: (a) computational model and boundary conditions; (b) displacement in the y-direction in Line 1–1 predicted by the FEM and the 4D lattice models; and (c) contour map of displacement in the y-direction, as obtained by the FEM and the 4D Lattice (IV) and 4D Lattice (I-m) models.

4D Lattice models are also shown together. The Poisson's ratios obtained for the 4D cubic lattices from hyperelasticity analysis cover nearly the entire experimental data set. However, the admissible range of stiffness parameters in the fourth dimension is limited by the physical stability of the corresponding lattice configurations, as shown the data specified by the 4D Lattice (I), Lattice (II), Lattice (III), Lattice (IV) and Lattice (I-m) models. Fig. 4 indicates that the 4D lattice spring model might be also applicable for cubic elastic materials. Nevertheless, considering the cubic and random lattice configurations, the admissible Poisson's range of the 4D lattice spring model covers a large range of engineering materials such as concrete and rock [19]. Future work on the 4D lattice spring model should focus on the development of more variable 4D lattice configurations and their corresponding influence on the mechanical responses, the development of a constitutive model that accounts for a material's nonlinearity, investigation of the influence of microstructure on the mechanical responses of materials, and experimental verification and development of high-performance computing.

3. Numerical examples

3.1. Elastic problems

To verify the 4D lattice spring model, we solved a boundary value problem with a complex geometry domain using different 4D lattices (see Fig. 5(a)). For all simulations, the elastic modulus and Poisson's ratio were set to 10 GPa and 0.1, respectively. Mechanical damping was used to obtain the corresponding elastic displacement solution. Five 4D lattice models were used to solve the same problem, and the results were compared with the corresponding FEM results. The 4D Lattice (I-m) model gave reasonable results compared with the FEM solution. Contour maps of displacements in the y-direction predicted by the FEM and by the 4D Lattice (IV) and 4D Lattice (I-m) models are shown in Fig. 5(b). It can be seen that the Lattice (I-m) model closely reproduces the displacement field of the

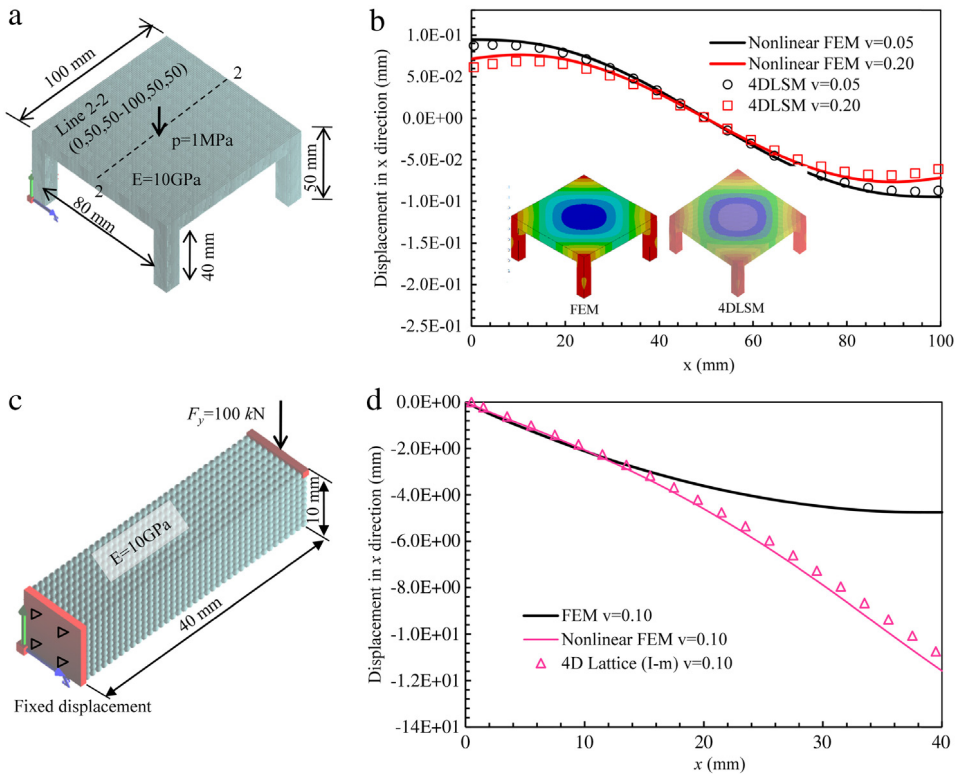

Fig. 6. Elastic problems solved by the 4D lattice spring model: (a) computational model of a table's deformation problem; (b) FEM and the 4D lattice spring model solutions with different Poisson's ratios; (c) computation of the nonlinear beam bending problem; and (d) nonlinear beam bending problem solved by linear FEM, nonlinear FEM and the 4D lattice spring model.

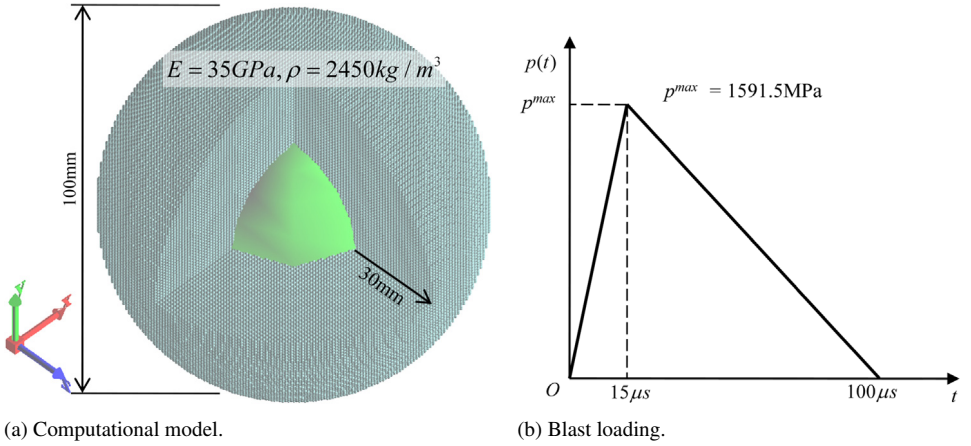

(a) Computational model. (b) Blast loading.

Fig. 7. Dynamic fracturing of a hollow sphere under blast loading: (a) computational model and boundary condition and (b) blasting represented as a triangle pressure loading.

FEM. This result indicates that the 4D lattice spring model can solve the boundary value problem of linear isotropic elasticity (the reason is provided in Section 2.4).

To demonstrate the capability of the 4D lattice spring model to recover different Poisson's ratios, tables with different Poisson's ratios under pressure were simulated (Fig. 6(a)). A comparison of the results of the displacement in the x-direction of line 2–2 along the table's surface predicted by the FEM with different Poisson's ratios with those predicted by the 4D Lattice (I-m) model is plotted in Fig. 6(b). The variation of the Poisson's ratio is captured by the

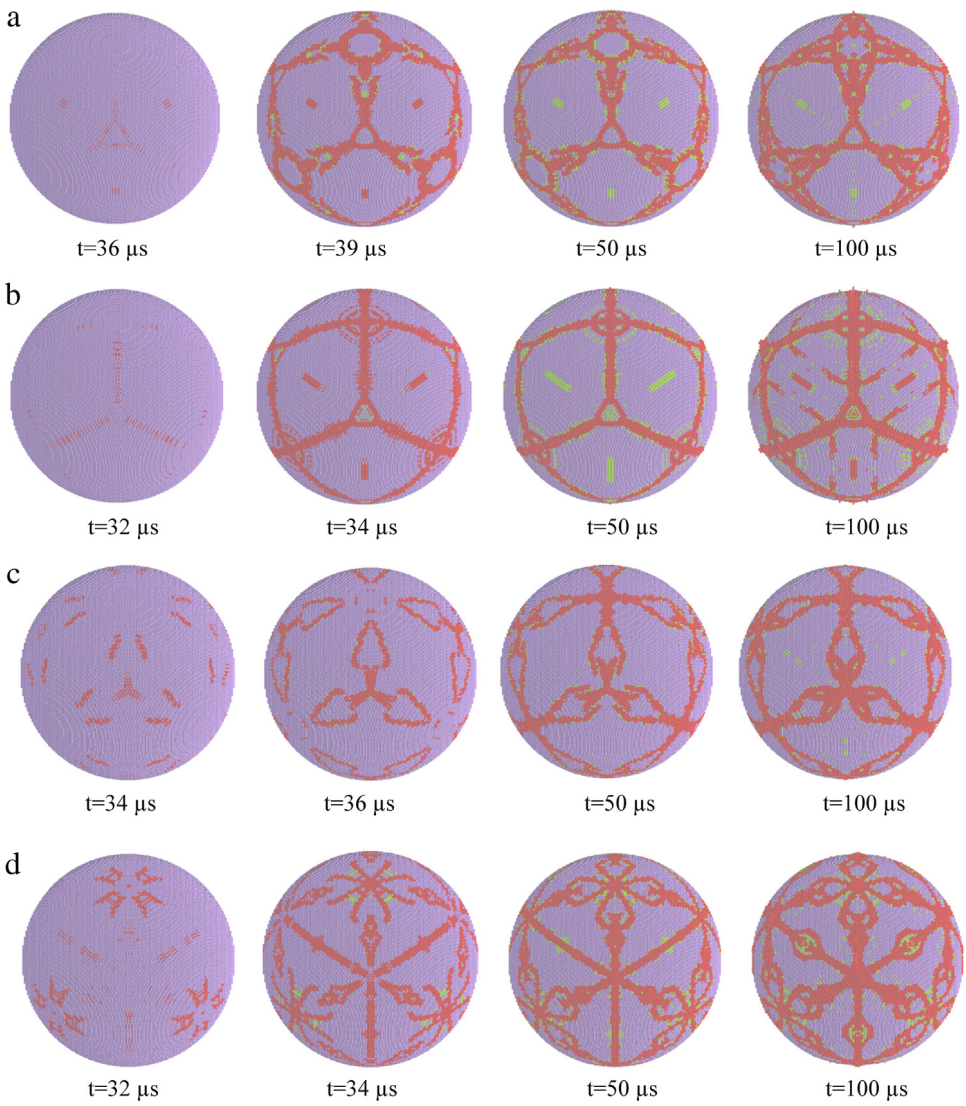

Fig. 8. Dynamic fracturing process of a hollow sphere under blasting loading with different Poisson's ratios and spring strengths (blue represents to the original solid, red indicates failure with particle opening, and green represents failure with particle closure), (a) $\upsilon = 0.05$, $u_n^* = 3.5 \times 10^{-3}$ mm, (b) $\upsilon = 0.05$, $u_n^* = 3.0 \times 10^{-3}$ mm, (c) $\upsilon = 0.23$, $u_n^* = 3.5 \times 10^{-3}$ mm, and (d) $\upsilon = 0.23$, $u_n^* = 3.0 \times 10^{-3}$ mm. (For interpretation of the references to colour in this figure legend, the reader is referred to the web version of this article.)

4D lattice spring model. We next considered a beam bending problem with large loading (Fig. 6(c)). Actual mechanical problems might involve both geometric and material nonlinearity. In the 4D lattice spring model, the geometric nonlinearity can be automatically considered since it adopts pure central force interaction which only depends on the current configuration of the computational model. As an example, in the following, a geometric nonlinear problem is solved by using the 4D lattice spring model. In Fig. 6(d), the corresponding displacement solution obtained by linear FEM, nonlinear FEM and the 4D lattice spring model are shown together. The results demonstrate that the 4D lattice spring model can capture the geometry nonlinearity automatically. Although we cannot experimentally prove that our world is 4D, the introducing extra dimension into a lattice spring model can lead to a more concise numerical model, which is still interesting. To consider the 4D interaction, one additional degree of freedom was introduced to each particle, which might increase the computational time slightly. To tackle this problem, the Open Multi-Processing (OpenMP) was adopted to parallelize the computer code of the 4D lattice spring model.

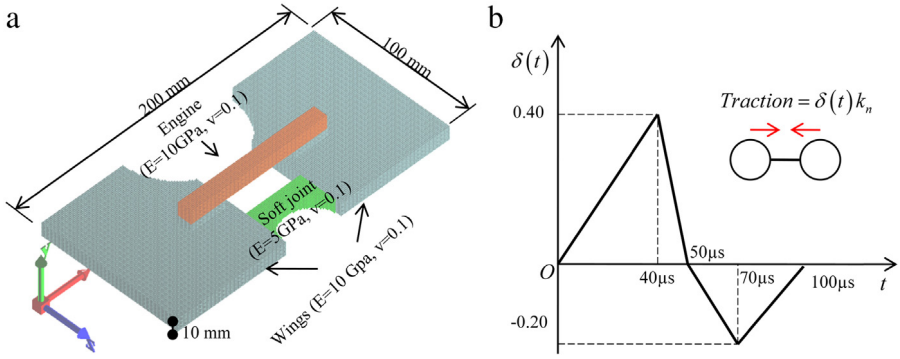

Fig. 9. Dynamic motion of a soft robot: (a) computational model and (b) input pulse for the engine material.

3.2. Dynamic fracturing of a hollow sphere under blasting

Fracture patterns of solids are of great interest in geosciences and engineering [20]. In the lattice spring model, the complex fracturing process can be represented as a series of spring-level failure events and is a promising, easily understood mechanical tool for investigating the mechanism of complex fracture. In this example, a simple brittle failure law is applied to base springs; that is, when the deformation between two particles is greater than the given threshold value, the spring will be broken and the corresponding non-self-mapped 4D interactions (β- and γ-interactions) will be removed from the calculation in the meantime. An example of dynamic fracturing of a hollow sphere under blasting is presented. The computational model is shown in Fig. 7(a) and consists of 490,432 particles with a diameter of 1 mm. The outer radius of the model is 50 mm, and the radius of the hollow spherical chamber is 20 mm. A blast loading shown in Fig. 7(b) is applied to the internal surface of the hollow sphere.

Numerical simulations with different strength parameters and Poisson's ratios were conducted; the corresponding results are shown in Fig. 8. Failure patterns with a sense of art were generated with a regular lattice using a regular failure criterion. During the simulation, the symmetry of the solution is ensured from the pure central interaction. The results lead to the conclusion that both the fracture energy (strength of spring) and the Poisson's ratio may strongly influence the surface fracture patterns of the sphere.

It should be mentioned that fragmentation of solids can also be well handled by using the Discontinuous Deformation Analysis (DDA) or the FEM with a cohesive joint model [21]. However, the 3D implementations of these models are complex and troublesome. Moreover, the 4D lattice spring model uses only one third of the degree of freedoms compared with its DDA and FEM counterparts (12 per numerical element), and might be more computationally efficient.

3.3. Dynamic motion of a soft robot

Development of a control technique that accounts for the material properties is regarded as one of the future research directions for soft robots [3]. This problem is a complex solid mechanics problem involving high nonlinear dynamic responses. In solid mechanics, the calculation of a rigid-body rotation tensor without dynamic inconsistency has been a recent research topic [22]. The 4D lattice spring model might be a promising candidate for such problems because it is free of polar decomposing calculations. For example, the polar decomposition is needed in the DLSM [23] to calculate the spring bond's shear deformation under a large deformation. Due to only the central force springs are used in the 4D lattice spring model, such operation can be avoided. As shown in Fig. 9(a), the robot consists of a combination of components: the wings, the joint and the engine simulated from a dynamic pulse input (see Fig. 9(b)).

The pulse is applied to the original spring linked mass particles of the engine according to a given prescribed function. The soft robot's length and width are 20 cm and 10 cm, respectively. During the simulation, the 4D lattice spring model did not use any artificial damping to stabilize the calculation. The simulation results presented in Fig. 10(a)–(c) show that dynamic deformation with large rigid rotation mixed with body deformation can be reasonably reproduced.

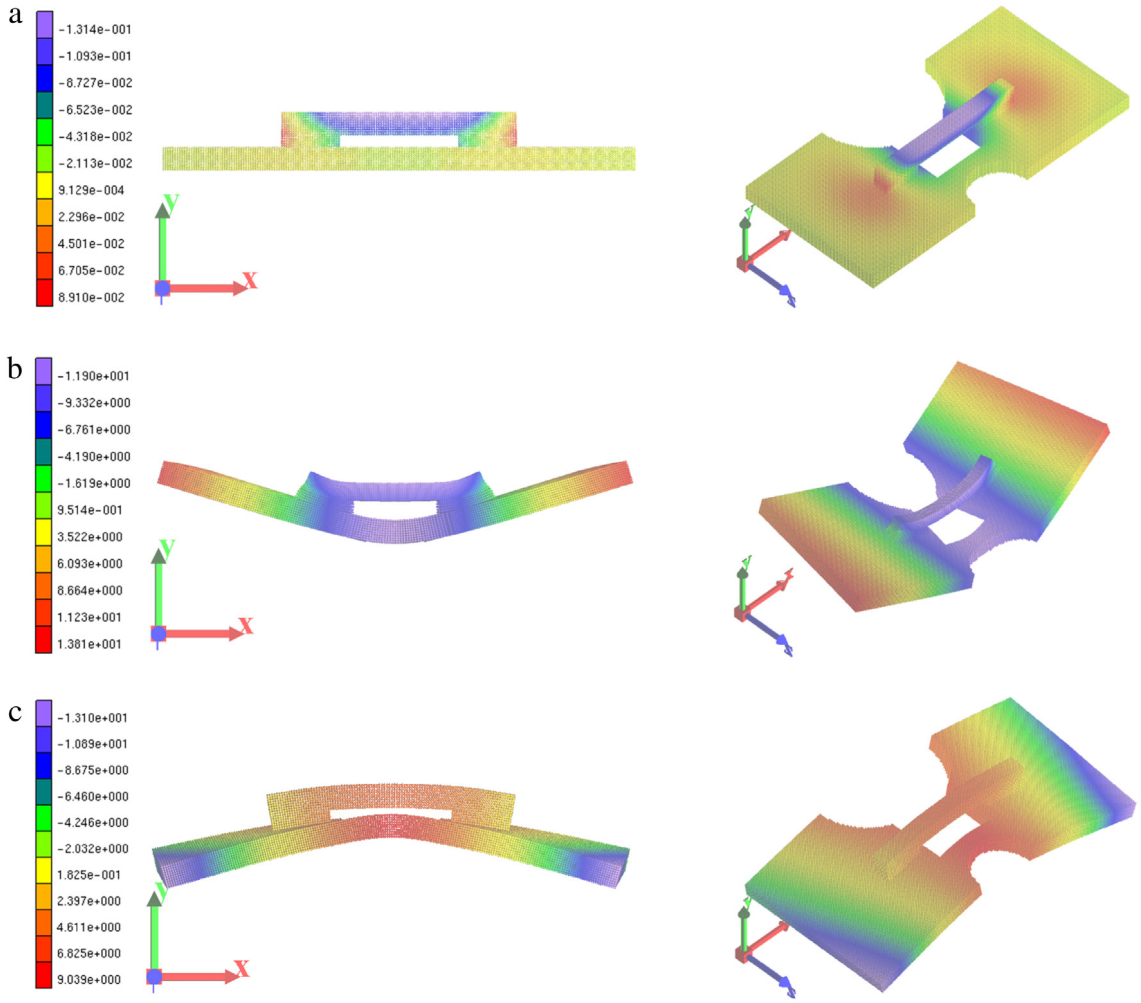

Fig. 10. Dynamic deforming of the soft robot predicted by the 4D lattice spring model (contour map of displacement in the y-direction): (a) $t = 1$ μs, (b) $t = 40$ μs, and (c) $t = 90$ μs.

4. Conclusions

We designed a 4D lattice spring model to overcome the Poisson's limitation of the classical lattice spring model by using the 4D interaction. The model has advantages in naturally modelling nonlinear dynamic responses of solids. Because the model adopts only the central interaction, it is free of special treatment of rigid body rotation and tensorial operations involved in the nonlinear analysis in the traditional top-to-bottom-based numerical methods such as FEM and NEM or incremental integration of the noncentral/nonlocal interaction in the bottom-to-top-based numerical methods such as DEM and modified lattice spring models. This work also demonstrates the possible benefits of introducing the extra-dimension concept from modern physics into solid mechanics. However, as a newly developed model, the 4D lattice spring model is still not perfect and needs further improvements. For example, specific constitutive models for plasticity and viscosity need to be developed for the 4D lattice spring model to solve actual engineering problems involving material nonlinearities such as slope failures and rock avalanches.

References

[1] G.N. Greaves, A.L. Greer, R.S. Lakes, T. Rouxel, Poisson's ratio and modern materials, Nat. Mater. 10 (2011) 823–837.
[2] K. Xia, A.J. Rosakis, H. Kanamori, J.R. Rice, Laboratory earthquakes along inhomogeneous faults: directionality and supershear, Science 308 (2005) 681–684.

[3] D. Rus, M.T. Tolley, Design, fabrication and control of soft robots, Nature 521 (2015) 467–475.
[4] R.W. Clough, The finite element method in plane stress analysis, in: Proc. Second ASCE Conf. Elec Compu, Pittsburg, PA, p. 345, 1960.
[5] J. Braun, M. Sambridge, A numerical method for solving partial differential equations on highly irregular evolving grids, Nature 376 (1995) 655–660.
[6] B.J. Alder, T.E., Studies in molecular dynamics, i, J. Chem. Phys. 31 (1959) 459.
[7] P.A. Cundall, O.D.L. Strack, A discrete numerical model for granular assemblies, Geotechnics 29 (1979) 47–65.
[8] A. Hrennikoff, Solution of problems of elasticity by the framework method, ASME J. Appl. Mech. 8 (1941) A619–A715.
[9] G. Caldarelli, C. Castellano, A. Petri, Criticality in models for fracture in disordered media, Physica A 270 (1999) 15–20.
[10] G. Lilliu, J.G.M. van Mier, 3D lattice type fracture model for concrete, Eng. Fract. Mech. 70 (2003) 927–941.
[11] G.-F. Zhao, J.N. Fang, J. Zhao, A 3D distinct lattice spring model for elasticity and dynamic failure, Int. J. Numer. Anal. Methods Geomech. 35 (2011) 859–885.
[12] H. Chen, E. Lin, Y. Jiao, Y. Liu, A generalized 2D non-local lattice spring model for fracture simulation, Comput. Mech. 54 (2014) 1541–1558.
[13] J.M. Overduin, P.S. Wesson, Phy. Rep. 183 (1997) 303–378.
[14] P.S. Wesson, Five-Dimensional Physics, World Sci. Pub., 2006.
[15] E. Rougier, A. Munjiz, N.W.M. John, Numerical comparison of some explicit time integration schemes used in DEM, FEM/DEM and molecular dynamics, Internat. J. Numer. Methods Engrg. 61 (2004) 856–879.
[16] H.J. Gao, P. Klein, Numerical simulation of crack growth in an isotropic solid with randomized internal cohesive bond, J. Mech. Phys. Solids 46 (1998) 187–218.
[17] Z.N. Zhang, X.R. Ge, Micromechanical consideration of tensile crack behavior based on virtual internal bond in contrast to cohesive stress, Theor. Appl. Fract. Mech. 43 (2005) 342–359.
[18] H.P.R. Frederikse, Elastic constants of single crystals, in: Handbook of Chemistry and Physics, eightyeighth ed., CRC Press, 2008.
[19] H. Gercek, Poisson's ratio values for rocks, Int. J. Rock. Mech. Min. Sci. 44 (2007) 1–13.
[20] T. Bai, D.D. Pollard, H. Gao, Explanation for fracture spacing in layered materials, Nature 403 (2000) 753–756.
[21] Y.Y. Jiao, H.Q. Zhang, X.L. Zhang, H.B. Li, Q.H. Jiang, A two-dimensional coupled hydromechanical discontinuum model for simulating rock hydraulic fracturing, Int. J. Numer. Anal. Methods Geomech. 39 (5) (2015) 457–481.
[22] G. Haller, Dynamic rotation and stretch tensors from a dynamic polar decomposition, J. Mech. Phys. Solids 86 (2016) 70–93.
[23] G.-F. Zhao, Development of the distinct lattice spring model for large deformation analyses, Int. J. Numer. Anal. Methods Geomech. 38 (10) (2014) 1078–1100.